LASER INTERFEROMETER GRAVITATIONAL WAVE OBSERVATORY
- LIGO -
CALIFORNIA INSTITUTE OF TECHNOLOGY
MASSACHUSETTS INSTITUTE OF TECHNOLOGY

Technical Note **LIGO-T1300633–v1** 2013/11/01

Quantum-noise reduction schemes for future advanced gravitational-wave detectors: Final report

Mikhail Korobko, Haixing Miao, and Yanbei Chen

California Institute of Technology
LIGO Project, MS 18-34
Pasadena, CA 91125
Phone (626) 395-2129
Fax (626) 304-9834
E-mail: info@ligo.caltech.edu

Massachusetts Institute of Technology
LIGO Project, Room NW22-295
Cambridge, MA 02139
Phone (617) 253-4824
Fax (617) 253-7014
E-mail: info@ligo.mit.edu

LIGO Hanford Observatory
Route 10, Mile Marker 2
Richland, WA 99352
Phone (509) 372-8106
Fax (509) 372-8137
E-mail: info@ligo.caltech.edu

LIGO Livingston Observatory
19100 LIGO Lane
Livingston, LA 70754
Phone (225) 686-3100
Fax (225) 686-7189
E-mail: info@ligo.caltech.edu

http://www.ligo.caltech.edu/

Abstract

Future advanced gravitational-wave detectors, such as Advanced LIGO, Advanced VIRGO, and KAGRA will be limited by noise due to quantum fluctuations in the light, around the most sensitive detection band 100Hz. There are two different approaches for improving the sensitivity: squeezing or canceling the noise by properly designing the input or output optics of the detector, and increasing the response to the gravitational-wave signal by modifying the test mass dynamics. In this project we take advantage of frequency-dependence of the optical spring to enhance the mechanical response in a broad frequency band.

1 Introduction

1.1 Standard Quantum Limit

Contemporary so-called second-generation gravitational-wave detectors, such as Advanced LIGO [1, 2], Advanced VIRGO [3], and KARGA [4], which are under construction now, will be quantum noise limited over the detection frequency band. At low frequencies, the radiation pressure noise dominates which is due to quantum fluctuation in the amplitude of the optical field; while at high frequencies, the shot noise dominates which arises from the phase fluctuation [5]. There is a trade-off between these two noises that is called the Standard Quantum Limit (SQL) [6]. For the linear position meter (the gravitational-wave interferometer is special case of it) the shot noise corresponds to the measurement noise and radiation pressure noise to the back-action noise.

The SQL is not an ultimate limit for measurement precision, there are two main approaches to overcoming the SQL: quantum noise cancellation and enhancement of the response of the test mass on the external force. The first one, Back-Action Evading (BAE) measurements, takes advantage of the correlation between the measurement noise and the back-action noise to evade the back action [7, 8, 9, 10, 11, 12]. Unfortunately any additional noise caused by optical losses in the system can destroy this correlation and eliminate the effect [13]. The second approach is based on the amplification of the gravitational wave signal by modifying test mass dynamics, and therefore it is more robust to the optical losses. This approach uses the dependence of the SQL on the response function of the test mass $\chi(\omega)$[14]:

$$S_F^{\mathrm{SQL}}(\omega) = 2\hbar|\chi^{-1}(\omega)|, \tag{1}$$

where ω is frequency of the signal and mechanical response is given by the ratio between mechanical displacement and the force $\chi(\omega) = x(\omega)/F(\omega)$. For the GW detector mirrors have resonant frequency around 1Hz, while the GW signal frequency is around 100Hz, so the test mass can be treated as free mass on these frequencies. The SQL for the free mass is:

$$S_F^{\mathrm{SQL}}(\omega) = 2\hbar m\omega^2 \tag{2}$$

This SQL can be surpassed by modifying the mechanical response (see Eq.(1)).

The purpose of this work is to investigate such modification of the response function using multiple optical springs. The outline of the report is the following: in the introductory part we explain the concept of optical spring in the section 1.2; review the study of negative optical inertia in section 1.3; discuss the idea of this research in section 1.4. Then we explain in details the nature of optical rigidity in the part 2 and finally describe a numerical approach to the problem in section 3.1.

1.2 Optical spring effect

As we mentioned above, the free mass SQL can be surpassed by modifying the mechanical response of the test mass. An example of such modification is transformation of a free mass to the oscillator by adding a spring. As shown in Fig. 1 (left) this modification enables to surpass the free mass SQL in the small region near the resonance.

Nevertheless according to the fluctuation-dissipation theorem losses in the mechanical spring cause the thermal noise, which is usually high at room temperature, so people are interested in other approaches for modifying the test-mass dynamics with

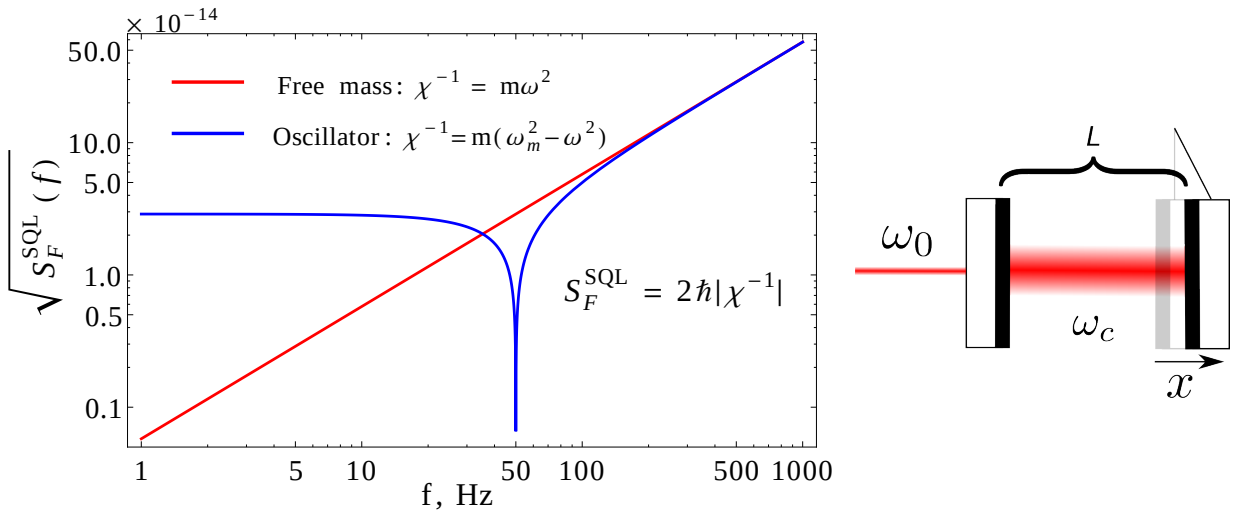

Figure 1: *(left)* SQL for the force in different systems: free mass (red) and oscillator with resonant frequency $\omega_m = 2\pi \times 50$ Hz (blue); *(right)* optical resonator with movable mirror which motion is being measured by laser.

low additional noise. We consider the optical spring effect that appears in the detuned optical cavity. We draw a classical analogy to explain the effect here while the rigorous derivation will be provided in the section 2. It is well-known that each photon colliding with a surface transfers a part of the momentum to it. Therefore a light beam creates an additional force on the surface which is proportional to the power of the beam. In the optical cavity the circulating power depends on the cavity detuning: if the cavity is tuned losses are minimal, but even small detuning creates significant reduction in the power (see Fig. 2). When the mirror displacement is small the power is proportional to it:

$$F_{\rm rp} = \frac{I}{c} = -\mathcal{K}x.$$

In other words, the detuning causes the appearance of the additional force, which is similar to the classical rigidity, and that is why this phenomenon is called optical spring [15, 16, 17].

As we show in the section 2 the optical rigidity term depends on the frequency:

$$\mathcal{K}(\omega) = \frac{mJ\delta}{(\gamma - i\omega)^2 + \delta^2},$$

where $\delta = \omega_c - \omega_0$ is detuning, ω_0 is laser frequency, ω_c is cavity resonant frequency, m is the mirror mass, γ is half-bandwidth, and renormalized power J is:

$$J = \frac{4\omega_0 I_c}{mcL}, \tag{3}$$

where L – cavity length, I_c - circulating power. The response function in this case

$$\chi_{\rm eff}(\omega) = \left[-m\omega^2 + \mathcal{K}(\omega)\right]^{-1}. \tag{4}$$

This response function is similar to the oscillator one, so optical spring can modify dynamics in the same way as mechanical spring, but it with less technical noise, because there is no more thermal noise caused by losses in the solid-state spring.

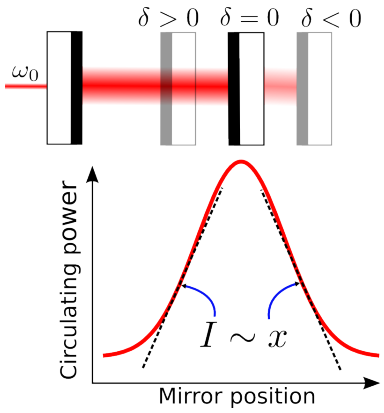

Figure 2: Dependence of the circulating power on the mirror position.

1.3 Double optical springs: negative inertia

In Ref.[18], Khalili et al. propose to use the frequency dependence of the optical spring to compensate the inertia term, and therefore to surpass the force SQL of the original test mass. When the frequency of interest is much smaller than detuning, we can expand the optical rigidity in Taylor series:

$$\mathcal{K} \approx \bar{\mathcal{K}} - i\Gamma_{\rm opt}\omega - m_{\rm opt}\omega^2 + \mathcal{O}(\omega^3), \tag{5}$$

where

$$\bar{\mathcal{K}} = \frac{mJ\delta}{\delta^2+\gamma^2}, \qquad \Gamma_{\rm opt} = -\frac{2mJ\gamma\delta}{(\gamma^2+\delta^2)^2}, \qquad m_{\rm opt} = -\frac{mJ\delta(\delta^2-3\gamma^2)}{(\delta^2+\gamma^2)^3}. \tag{6}$$

Since $\bar{\mathcal{K}}, \Gamma_{\rm opt}, m_{\rm opt}$ depend only on cavity bandwidth, cavity detuning and renormalized optical power, we can tune the $m_{\rm opt}$ in such a way to compensate the positive inertia of the test mass. By combining two optical springs we can cancel the constant $\bar{\mathcal{K}}_{1,2}$ and inertia terms:

$$\bar{\mathcal{K}}_1 + \bar{\mathcal{K}}_2 = 0, \qquad m + m_{\rm opt,1} + m_{\rm opt,2} = 0. \tag{7}$$

This cancellation significantly reduces the force SQL compared to the free mass one (Eqs. (1),(4),(5)):

$$\frac{[S_{\rm F}^{\rm SQL}]_{\rm modified}}{[S_{\rm F}^{\rm SQL}]_{\rm free\ mass}} = \left|\frac{[\chi(\omega)_{\rm modified}]}{m\omega^2}\right| \approx \left|\frac{|m_{\rm opt}| - m}{m}\right|. \tag{8}$$

By tuning $|m_{\rm opt}| \to m$, we can make the ratio much smaller than unity.

This approach works at low frequencies and breaks down at high frequencies because we have to take into account higher-order terms in the Taylor series (5) and that limits us in achieving better sensitivity a broad frequency band.

1.4 Multiple optical springs

The idea of the negative inertia can be generalized: more optical springs may provide more significant modification of the dynamics, even cancel the significant part of the

mechanical inertia in a broad frequency range. The goal is to obtain the independence of the inverse response function on the frequency in some frequency range:

$$\chi_{\rm eff}^{-1}(\omega) = -m\omega^2 + \sum_{i=1}^{N} \mathcal{K}_i(\omega) \approx \text{const.} \tag{9}$$

We need this term to be some nonzero constant, because otherwise the response would be infinite, and any small fluctuation around zero in the inverse response function would create a huge noise in the response. Making the constant to be small, but nonzero will relive us from this issue.

When the test mass response is frequency dependent we can only touch the SQL on one frequency with given power. Unlike that if the response is constant the SQL will be constant in the range as well, and we will be able to reach it without changing the power in any point over this frequency range.

In order to understand the approach to the solution we provide a more quantitative description of the optical spring in the next section.

2 Optical rigidity

The interaction Hamiltonian of a cavity with one movable mirror and an input laser:

$$\hat{\mathcal{H}} = \frac{1}{2} m\omega_m^2 \hat{x}^2 + \frac{\hat{p}^2}{2m} + \hbar\omega_c \hat{c}^\dagger \hat{c} + \hbar G_0 \hat{x} \hat{c}^\dagger \hat{c} + i\hbar\sqrt{2\gamma}\big(\hat{a}\hat{c}^\dagger e^{-i\omega_0 t} - \hat{a}^\dagger \hat{c} e^{-i\omega_0 t}\big). \tag{10}$$

The first term is free Hamiltonian for the mechanical mode ($[\hat{x}, \hat{p}] = i\hbar$). The second one describes the cavity mode with annihilation operator $\hat{c}$ and commutator $[\hat{c}, \hat{c}^\dagger] = 1$. The third is interaction between the oscillator and light with optomechanical coupling constant $G_0 = \omega_0/L$. The last term describes interaction of the pump $\hat{a}$ with the field in the cavity with half-bandwidth γ.

This Hamiltonian can be linearized if we assume the pump has a large amplitude so we can apply unitary transformation to have $\hat{c}$ referring to the vacuum state:

$$\hat{c} \to \bar{c} + \hat{c}, \qquad \hat{c} \ll \bar{c}.$$

Then in the rotating frame of laser frequency we get linearized Hamiltonian:

$$\hat{\mathcal{H}} = \frac{1}{2} m\omega_m^2 \hat{x}^2 + \frac{\hat{p}^2}{2m} + \hbar\delta \hat{c}^\dagger \hat{c} + \hbar G_0 \hat{x}(\hat{c}^\dagger \bar{c} + \bar{c}^* \hat{c}) + i\hbar\sqrt{2\gamma}\big(\hat{a}\hat{c}^\dagger - \hat{a}^\dagger \hat{c}\big), \tag{11}$$

where $\delta = \omega_c - \omega_0$ is detuning. We can always choose a phase for the $\bar{c}$ to be a real value, so we simplify the equation by the substitution $g = G_0\bar{c}$.

The Heisenberg equation is [19]:

$$\dot{\hat{c}} = -\frac{i}{\hbar}[\hat{c}, \hat{\mathcal{H}}] - \gamma \hat{c}. \tag{12}$$

We find:

$$\dot{\hat{c}} + (\gamma + i\delta)\hat{c} = -ig\hat{x} + \sqrt{2\gamma}\hat{a}, \tag{13}$$

For the output signal we have [19]:

$$\hat{b} = -\hat{a} + \sqrt{2\gamma}\hat{c}. \tag{14}$$

We can derive the equation of motion the mechanical mode:

$$\begin{aligned}\dot{\hat{x}} &= \frac{\hat{p}}{m} \\ \dot{\hat{p}} + \gamma_m \hat{p} &= -m\omega_m^2 \hat{x} + \hbar g(\hat{c}^\dagger + \hat{c}) + \hat{\zeta}_{\rm th}\end{aligned} \tag{15}$$

where $\hat{\zeta}_{\rm th}$ is Brownian thermal force with correlation function

$$\langle \hat{\zeta}_{\rm th}(t)\hat{\zeta}_{\rm th}(t')\rangle = 2m\gamma_m k_B T\delta(t-t').$$

Equations (13) and (15) can be solved in the frequency domain, which gives

$$\hat{c}(\omega) = \frac{g\hat{x}(\omega) + i\sqrt{2\gamma}\hat{a}(\omega)}{\omega - \delta + i\gamma} \tag{16}$$

$$\hat{x}(\omega) = \frac{\hbar g(\hat{c}^\dagger + \hat{c}) + \hat{\zeta}_{\rm th}}{m(\omega_m^2 - \omega^2 - i\gamma_m\omega_m)} \tag{17}$$

The radiation pressure term here is:

$$\begin{aligned}F_{\rm rp} = \hbar g(\hat{c}^\dagger + \hat{c}) = \hbar g^2 \hat{x}(\omega)\left(\frac{1}{\omega - \delta + i\gamma} - \frac{1}{\omega + \delta + i\gamma}\right) + \\ + \hbar g i\sqrt{2\gamma}\left(\frac{\hat{a}^\dagger}{\omega + \delta + i\gamma} + \frac{\hat{a}}{\omega - \delta + i\gamma}\right).\end{aligned} \tag{18}$$

The second term is noise, and the first one linearly depends on the mechanical displacement:

$$F_{\rm rp} = -\mathcal{K}(\omega)\hat{x}(\omega) + \hat{F}_n(\omega). \tag{19}$$

Here $\mathcal{K}(\omega)$ is optical rigidity:

$$\mathcal{K}(\omega) = \frac{2\hbar g^2 \delta(\omega)}{(\omega - \delta + i\gamma)(\omega + \delta + i\gamma)}. \tag{20}$$

Recalling the definition of the renormalized power (3), relation of the circulating power to the total energy stored in the cavity

$$\mathcal{E} = \hbar\omega_0 \bar{c}^2 = \frac{2L}{c} I_c$$

and coupling constant $g = \bar{c}\omega_0/L$, we can put this term in the form we introduced it before:

$$\mathcal{K}(\omega) = \frac{mJ\delta}{(\gamma - i\omega)^2 + \delta^2}. \tag{21}$$

The radiation pressure noise term F_n describes the quantum fluctuations of the optical field:

$$F_n = 2\hbar g\sqrt{\gamma}\frac{\hat{a}_1(\gamma - i\omega) + \delta\hat{a}_2}{(\omega - \delta + i\gamma)(\omega + \delta + i\gamma)}, \tag{22}$$

with two quadratures

$$\hat{a}_1 = \frac{\hat{a} + \hat{a}^\dagger}{\sqrt{2}}, \hat{a}_2 = \frac{\hat{a} - \hat{a}^\dagger}{i\sqrt{2}}.$$

We can evade this noise by properly combining the outputs from carrier measuring the noise, and auxiliary sensing beam measuring the signal [20].

The optical rigidity term can be considered as a part of new effective response function:

$$\chi_{\text{eff}}^{-1}(\omega) = -m\omega^2 + \mathcal{K}(\omega). \tag{23}$$

Then the dynamics of the oscillator can be described by:

$$\hat{x}(\omega) = \chi_{\text{eff}}(\omega)[\hat{F}_n + \hat{\zeta}_{\text{th}}] \tag{24}$$

Following the logic of the first section, we can now investigate a way of combining multiple springs to modify the dynamics in the desired way.

3 Multiple Optical Springs

3.1 Vector fitting

Each optical spring term is nonlinear function of the frequency and other parameters: power, detuning and half-bandwidth. The analytical solution of the equation (9) is complicated (if possible at all). Nevertheless this problem can be treated in a different way - as data fitting problem. Then we can find numerically the parameters of this fitting. However, nonlinear fitting requires a lot of computing resources and good optimization algorithm, so it is important to choose appropriate procedure.

The optical spring term has the same shape as commonly used in physics response function. We can use this feature and implement special procedure, called vector fitting (VF) [21, 22]. Usually the response function has several poles, so the procedure estimates these poles a_i and residues c_i:

$$f(s) = \sum_{i=1}^{N} \frac{c_i}{s - a_i} + d + sh, \tag{25}$$

where $s = i\omega$; d and h are constants; c_i, a_i are either real or complex conjugate pairs. The procedure iteratively runs two steps: relocates poles on the new place and estimates residues. This algorithm was created for power system transients modeling, but it can be used in our task as well, because the shape of the optical rigidity term is similar to the one VF requires. It becomes more clear if we represent the optical spring term as

$$\mathcal{K}(s) = \frac{mJ\delta}{(\gamma - s)^2 + \delta^2} = \frac{mJ\delta}{(\gamma + i\delta - s)(\gamma - i\delta - s)} = \frac{m}{2}\left(\frac{-iJ}{s - (\gamma + i\delta)} + \frac{iJ}{s - (\gamma - i\delta)}\right). \tag{26}$$

By setting

$$a_i = \gamma - i\delta, \qquad a_{i+1} = a_i^*, \qquad c_i = iJ, \qquad c_{i+1} = c_i^* = -iJ, \qquad h = 0, d = 0, \tag{27}$$

and assuming data to be $f(s) = ms^2 + \text{const}$ (see Eq.(9)) we can use VF algorithm with some modifications, which we discuss below.

3.1.1 Original algorithm

Originally algorithm identifies the the parameters of the response (25). This method works recursively, each iteration includes two steps: in the first step it estimates poles of the function and in the second step it uses least squares (LSQ) method to fit linear function of residuals to the data. More precisely, first we choose some random set of starting poles $\bar{a}_i$ and multiply $f(s)$ on some unknown function with same poles $\bar{a}_i$:

$$\sigma(s) = \sum_{i=1}^{N} \frac{\tilde{c}_i}{s - \bar{a}_i} + 1, \tag{28}$$

and thus get an approximation to the rescaled function $\sigma(s)f(s)$ with same poles as these two:

$$(\sigma f)(s) = \sum_{i=1}^{N} \frac{\tilde{c}_i}{s - \bar{a}_i} + d + sh. \tag{29}$$

Combining two equations (28), (29), we get:

$$\sum_{i=1}^{N} \frac{c_i}{s - \bar{a}_i} + d + sh \approx (\sum_{i=1}^{N} \frac{\tilde{c}_i}{s - \bar{a}_i} + 1) f(s), \tag{30}$$

where unknowns are $c_i, \tilde{c}_i, d, h$. Parameters are complex conjugated pairs:

$$c_i = c' + ic'', \quad c_{i+1} = c' - ic'', \quad a_i = a' + ia'', \quad a_{i+1} = a' - ia''.$$

Taking it into account, we can write down the overdetermined linear problem $Ax = b$ where x is vector of unknown parameters and

$$A_k x = b_k, \qquad b_k = f(s_k),$$

$$A_k = \left[\dots \quad \tfrac{1}{s_k - a_i} + \tfrac{1}{s_k - a_i^*} \quad \tfrac{i}{s_k - a_i} - \tfrac{i}{s_k - a_i^*} \quad \dots \quad 1 \quad s_k \quad \tfrac{-f(s)}{s_k - a_i} + \tfrac{-f(s)}{s_k - a_i^*} \quad \tfrac{-if(s)}{s_k - a_i} - \tfrac{-if(s)}{s_k - a_i^*}, \right] \tag{31}$$

$$x = \left[\dots \quad c' \quad c'' \quad \dots \quad d \quad h \quad \dots \quad \tilde{c}' \quad \tilde{c}'' \quad \dots .\right]^T \tag{32}$$

This problem can be solved via the method of least squares and then we can use these residues for finding new poles. If we rewrite our functions in the following form:

$$(\sigma f)(s) = h \frac{\prod_{i=1}^{N+1} (s - z_i)}{\prod_{i=1}^{N} (s - \bar{a}_i)}, \qquad \sigma(s) = \frac{\prod_{i=1}^{N} (s - \tilde{z}_i)}{\prod_{i=1}^{N} (s - \bar{a}_i)}, \tag{33}$$

$$f(s) = \frac{(\sigma f)(s)}{\sigma(s)} = h \frac{\prod_{i=1}^{N+1} (s - z_i)}{\prod_{i=1}^{N} (s - \tilde{z}_i)}. \tag{34}$$

Thus zeros of σ are poles of $f(s)$. Zeros a_i are eigenvalues of the matrix $A - bc^T$, where A is a diagonal matrix of initial poles, b is column vector of ones and c is vector of residues $\tilde{c}_i$.

If the initial poles are correct then the new poles (zeros of $\sigma(s)$) become equal to the initial poles and that $\sigma(s) = 1$. Therefore if we use new poles as starting poles for the new iteration the procedure will converge.

3.1.2 Modified algorithm

In our case we have to modify the algorithm to fit our requirements. The differences to the original algorithm are:

- we should restrict our parameters c_i to be pure imaginary, which is equivalent to setting $c_i' = 0$ in the algorithm;
- to make parameters a_i to have both real and imaginary part we can throw away real poles;

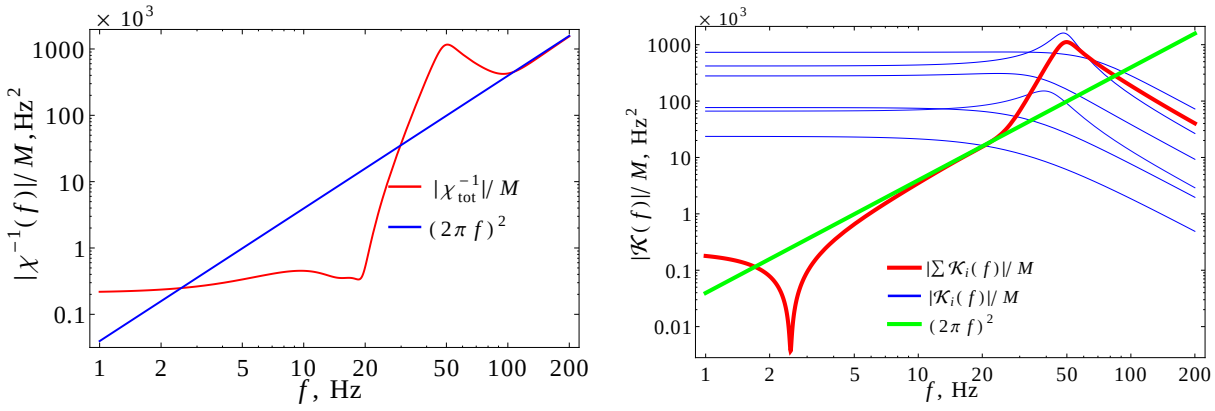

Figure 3: (left) Modified response (red) compared to that of the free mass (blue) for 6 springs; (right) contribution of each spring to the response.

P,W	8.8×10^5	1.2×10^5	5.1×10^5	1.7×10^5	1.4×10^5	2.56112×10^6
δ, Hz	304.8	-251.3	192.2	121.5	37.9	-299.4
γ, Hz	40.4	58.1	121.8	160.9	178.6	254.7

Table 1: Parameters of the optical springs

- the power cannot be negative, so when we get negative values in LSQ we should change both signs of detuning and power;
- the total circulating power should have some reasonable value, so we can argue that it should be rather close to the one advanced LIGO has ($800kW$). That means 10MW is fine, but 100MW is too much. In order to bound its value we can implement bounded value least squares (BVLS)[23, 24]

This modified algorithm gives almost flat response function in a broad band from 1Hz to 20Hz. As an example oin Fig. 3 we show such a response achieved by 6 optical springs with total power of 4.4MW and reasonable parameters (see Table 1). The fact that the curve is not flat in the region of the interest we refer to the poor convergence of the algorithm. As stated in [22] the original algorithm [21] that we use in our work has some convergence issues - in some cases the poles cannot be relocated on a long distance. However increasing the number of springs it is possible to achieve a line in a region from 1Hz to 20Hz with 7 springs (see left part of Fig.4) or even in a broader region from 1Hz to 100Hz with 15 springs (see right part of Fig.4).

4 Discussion and future plans

In the work we achieve the constant response function in a broad frequency band from 1Hz to 20Hz. We show that we can use several (6 and 7 in examples) optical springs of total power less than 10MW to have this effect. One can also broaden the range by adding more springs. This response function will give us the flat SQL, which can be achieved in any point with the same power (if we sense the effective response by another probe beam).

Nevertheless, this result requires detailed investigation and we have the following objectives for the future research:

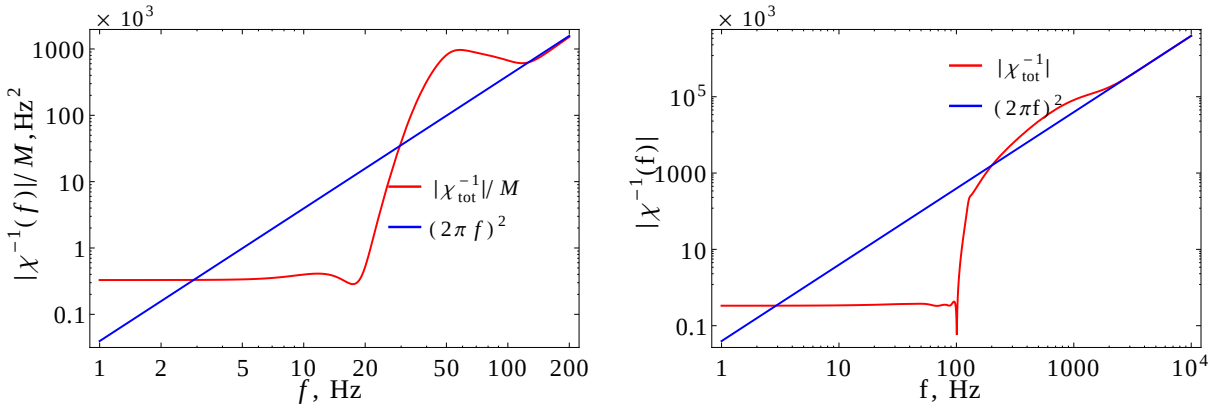

Figure 4: Modified response (red) comparing to the free mass (blue): 7 optical springs in the region (1 to 20)Hz *(left)* ; 15 optical springs in the region (1 to 100)Hz *(right)*

- The next objective is to implement an improved version of the algorithm to achieve better convergence and improve the pole relocation properties [22].
- Though we increase the response, it is not clear how multiple optical springs will affect the output spectral density (see derivation of spectral density in Appendix A). There are two ways of obtaining the information about the force: we can either combine carriers creating these springs in an optimal way (see Appendix B)) and get the information directly from them, or add one measurement beam, leaving the springs to be only for dynamics modification. The second approach can be preferable, because we can read information about noises from output of carrier light as well and then subtract it from measured data (perform partial back-action evasion [20]).
- The other interesting issue to investigate is general analytical description of the task. In the limit of infinite amount of springs it can be possible to consider not the sum of springs, but integral over parameter space, and find poles on the complex plane using Cauchy integral theorem and investigate their properties (in Appendix C we give an outline and some examples).

5 Acknowledgments

I would like to acknowledge my mentors, Haixing Miao and Yanbei Chen, for invaluable assistance in this work, Huan Yang, Nikita Voronchev and Nikita Vostrosablin for fruitful discussion, and also Caltech, SURF Program and LIGO Project for providing the financial support and organization of this summer work in Caltech.

References

[1] www.advancedligo.mit.edu.

[2] G.M.Harry (for the LIGO Scientic Collaboration). Advanced ligo: the next generation of gravitational wave detectors. *Classical and Quantum Gravity*, 27:084006, 2010.

[3] http://wwwcascina.virgo.infn.it/advirgo/.

[4] http://gwcenter.icrr.u-tokyo.ac.jp/en/.

[5] CM Caves. Quantum-mechanical noise in an interferometer. *Physical Review D*, 1981.

[6] V.B.Braginsky, F.Ya.Khalili. *Quantum Measurement*. Cambridge University Press, 1992.

[7] H.J.Kimble, Yu.Levin, A.B.Matsko, K.S.Thorne and S.P.Vyatchanin. Conversion of conventional gravitational-wave interferometers into QND interferometers by modifying their input and/or output optics. *Physical Review D*, 65:22002, 2001.

[8] W.G.Unruh. In P.Meystre and M.O.Scully, editor, *Quantum Optics, Experimental Gravitation, and Measurement Theory*, page 647. Plenum Press, New York, 1982.

[9] F.Ya.Khalili. No Title. *Doklady Akademii Nauk*, 294:602–604, 1987.

[10] M.T.Jaekel and S.Reynaud. Quantum limits in interferometric measurements. *Europhysics Letters*, 13:301, 1990.

[11] A.F.Pace, M.J.Collett and D.F.Walls. *Physical Review A*, 47:3173, 1993.

[12] S.P.Vyatchanin and A.B.Matsko. Quantum variation scheme of measurement of force and compensation of back action in intereferometric meter of position. *Sov. Phys. JETP*, 83:690–697, 1996.

[13] Yanbei Chen, Stefan L Danilishin, Farid Ya. Khalili, and Helge Müller-Ebhardt. QND measurements for future gravitational-wave detectors. page 22, October 2009.

[14] S. L. Danilishin. Quantum Measurement Theory in Gravitational-Wave Detectors. *Living Rev. Relativity*, 2012.

[15] H.Rehbein, H.Mueller-Ebhardt, K.Somiya, S.L.Danilishin, R.Schnabel, K.Danzmann, Y.Chen. Double optical spring enhancement for gravitational wave detectors. *Physical Review D*, 78:062003, 2008.

[16] Alessandra Buonanno and Yanbei Chen. Laser-interferometer gravitational-wave optical-spring detectors. *Classical and Quantum Gravity*, (July 2001):8–13, 2002.

[17] Alessandra Buonanno and Yanbei Chen. Signal recycled laser-interferometer gravitational-wave detectors as optical springs. *Physical Review D*, 64(ii):1–42, July 2002.

[18] Farid Khalili, Stefan Danilishin, and H Müller-Ebhardt. Negative optical inertia for enhancing the sensitivity of future gravitational-wave detectors. *Physical Review D*, 1:1–7, 2011.

[19] D.F. Walls and G.J. Milburn. Quantum Optics, 2008.

[20] WZ Korth, Haixing Miao, Thomas Corbitt, and GD Cole. A quantum radiation pressure noise-free optical spring. *arXiv preprint arXiv: ...*, pages 1–10, 2012.

[21] B Gustavsen and A Semlyen. Rational approximation of frequency domain responses by vector fitting. *Power Delivery, IEEE Transactions ...*, 14(3):1052–1061, 1999.

[22] Bjø rn Gustavsen. Improving the pole relocating properties of vector fitting. *Power Delivery, IEEE Transactions on*, 21(3):1587–1592, 2006.

[23] CL Lawson and RJ Hanson. *Solving least squares problems*. 1974.

[24] http://lib.stat.cmu.edu/general/bvls.

A Spectral density

In this section we derive the output spectral density of the system with one carrier. In the following analysis we introduce the classical force G acting on the system. From Eqs.(14),(16) we can derive the two-photon output quadratures:

$$\hat{\mathbf{b}}(\omega) = \mathbb{R}\hat{a}(\omega) + 2\sqrt{\gamma}\mathbb{L}\hat{X}(\omega), \tag{35}$$

where

$$\mathbb{L} = \frac{1}{\mathcal{D}(\omega)}, \begin{bmatrix} \gamma - i\omega & -\delta \\ \delta & \gamma - i\omega \end{bmatrix}, \tag{36}$$

$$\mathcal{D}(\omega) = (\gamma - i\omega)^2 + \delta^2, \tag{37}$$

$$\hat{X}(\omega) = \bar{c}\frac{k_0\hat{x}(\omega)}{\sqrt{\tau}} \begin{bmatrix} 0 \\ 1 \end{bmatrix}, \qquad k_0 = \omega_0/c, \qquad \tau = L/c, \tag{38}$$

$$\mathbb{R} = 2\gamma\mathbb{L} - \mathbb{I}. \tag{39}$$

and $\bar{c}$ is amplitude of the classical field in the cavity. In the single-mode approximation the field in the cavity is:

$$\hat{\mathbf{c}}(\omega) = \frac{\mathbb{L}(\omega)}{\sqrt{\tau}} \left(\sqrt{\gamma}\hat{a} + \hat{X}(\omega)\right). \tag{40}$$

Thus the back-action force is:

$$F_{\mathrm{BA}} = \frac{2\hbar k_0 \bar{c}}{\sqrt{\tau}}\hat{\mathbf{c}}(\omega) \begin{bmatrix} 1 \\ 0 \end{bmatrix}^T = F_n - \mathcal{K}(\omega)\hat{x}(\omega), \tag{41}$$

where

$$F_n = \frac{2\hbar k_0 \bar{c}\sqrt{\gamma}}{\sqrt{\tau}}\mathbb{L}(\omega) \begin{bmatrix} 1 \\ 0 \end{bmatrix}^T, \tag{42}$$

$$\mathcal{K}(\omega) = \frac{mJ\delta}{\mathcal{D}(\omega)}, \qquad J = \frac{4\omega_0 I_c}{mcL} = \frac{4\hbar k_0^2 \bar{c}^2}{m\tau}, \tag{43}$$

which is exactly what we get in the equation (18). As we mentioned before, the optical spring term $\mathcal{K}$ can be treated as part of the effective response function, thus the dynamics of the system is:

$$\hat{x}(\omega) = \chi_{xx}^{\mathrm{eff}}(\omega)\left[\hat{F}_n + G(\omega)\right], \tag{44}$$

where G is external classical force and effective susceptibility is:

$$\chi_{xx}^{\mathrm{eff}\,-1} = \chi_{xx}^{-1} + \mathcal{K}(\omega) = -m(\omega^2 + i\gamma_m\omega - \omega_m^2) + \mathcal{K}(\omega). \tag{45}$$

In general the system can be described by the system:

$$\begin{cases} \hat{\mathcal{O}}(\omega) = \hat{\mathcal{O}}^{(0)}(\omega) + \chi_{OF}(\omega)\hat{x}(\omega) \\ \hat{F}(\omega) = \hat{F}^{(0)}(\omega) + \chi_{FF}\hat{x}(\omega) \\ \hat{x}(\omega) = \chi_{xx}^{\mathrm{eff}}(\hat{F}_n(\omega) + G(\omega)) \end{cases} \tag{46}$$

where $\hat{\mathcal{O}}$ is output from the measurement system and $\hat{F}$ is the radiation pressure force (back-action). The measurement result we get by applying measurement operator $\mathbf{H}$ to the output $\hat{b}$. In case of the homodyne detection:

$$\hat{\mathcal{O}}(\omega) = \mathbf{H}^{\mathrm{T}}\hat{\mathbf{b}}(\omega) = \begin{bmatrix}\cos\zeta \\ \sin\zeta\end{bmatrix}^{\mathrm{T}} \begin{bmatrix}\hat{b}_c \\ \hat{b}_s\end{bmatrix} = \hat{b}_c\cos\zeta + \hat{b}_s\sin\zeta. \tag{47}$$

The parameters of the general description derived above in our case are:

$$\chi_{OF}(\omega) = 2\frac{k_0\sqrt{\gamma}}{\sqrt{\tau}}\mathbf{H}^{\mathrm{T}}\mathbb{L}(\omega)\bar{c}\begin{bmatrix}0\\1\end{bmatrix}, \tag{48}$$

$$\hat{\mathcal{O}}^{(0)} = \mathbf{H}^{\mathrm{T}}\mathbb{R}\hat{a}, \tag{49}$$

$$\chi_{FF}(\omega) = -\mathcal{K}(\omega), \tag{50}$$

$$\hat{F}^{(0)} = \frac{2\hbar k_0\bar{c}\sqrt{\gamma}}{\sqrt{\tau}}\begin{bmatrix}1\\0\end{bmatrix}^{T}\mathbb{L}(\omega)\hat{a}. \tag{51}$$

The system (46) can be resolved:

$$\hat{\mathcal{O}}(\omega) = \hat{\mathcal{O}}^{(0)}(\omega) + \frac{\chi_{xx}^{\mathrm{eff}}\chi_{OF}}{1-\chi_{xx}^{\mathrm{eff}}\chi_{FF}}\left[G(\omega) + \hat{F}^{(0)}\right]. \tag{52}$$

This equation can be renormalized to the more convenient form. In particular, we can consider the signal as sum of the classical force and some noise:

$$\hat{\mathcal{O}}^{F}(\omega) = \hat{\mathcal{N}}^{F} + G(\omega) = \frac{\hat{\mathcal{X}}}{\chi_{xx}^{\mathrm{eff}}(\omega)} + \hat{\mathcal{F}}(\omega) + G(\omega), \tag{53}$$

where

$$\hat{\mathcal{X}}(\omega) = \frac{\hat{\mathcal{O}}^{(0)}(\omega)}{\chi_{OF}(\omega)} = \sqrt{\frac{\hbar}{\gamma m J}}\frac{\mathcal{D}(\omega)}{\mathbf{H}^{\mathrm{T}}\mathbf{D}}\mathbf{H}^{\mathrm{T}}\mathbb{R}\hat{a}, \tag{54}$$

$$\mathbf{D}(\omega) = \mathcal{D}(\omega)\mathbb{L}(\omega)\begin{bmatrix}0\\1\end{bmatrix} = \begin{bmatrix}-\delta\\ \gamma - i\omega\end{bmatrix}, \tag{55}$$

$$\hat{\mathcal{F}}(\omega) = \hat{F}_n = \sqrt{mJ\hbar\gamma}\begin{bmatrix}1\\0\end{bmatrix}^{\mathrm{T}}\mathbb{L}(\omega)\hat{a}. \tag{56}$$

The spectral density of the output is:

$$S^{F}(\omega) = \frac{S_{\mathcal{X}\mathcal{X}}}{|\chi_{xx}^{\mathrm{eff}}|^2} + S_{\mathcal{F}\mathcal{F}} + 2\Re\left\{\frac{S_{\mathcal{X}\mathcal{F}}}{\chi_{xx}^{\mathrm{eff}}}\right\}, \tag{57}$$

with corresponding spectral densities:

$$S_{\mathcal{X}\mathcal{X}} = \frac{\hbar}{4\gamma m J}\frac{|\mathcal{D}(\omega)^2|}{\mathbf{H}^{\mathrm{T}}\mathbf{D}\mathbf{D}^{\dagger}\mathbf{H}}\mathbf{H}^{\mathrm{T}}\mathbb{R}\mathbb{R}^{\dagger}\mathbf{H} = \frac{\hbar}{4\gamma m J}\frac{1}{\left|\mathbf{H}^{\mathrm{T}}\mathbb{L}\begin{bmatrix}1\\0\end{bmatrix}\right|^2}, \tag{58}$$

$$S_{\mathcal{F}\mathcal{F}} = \gamma m\hbar J\begin{bmatrix}1\\0\end{bmatrix}^{\mathrm{T}}\mathbb{L}\mathbb{L}^{\dagger}\begin{bmatrix}1\\0\end{bmatrix}, \tag{59}$$

$$S_{\mathcal{X}\mathcal{F}} = \frac{\hbar}{2}\frac{\mathcal{D}(\omega)}{\mathbf{H}^{\mathrm{T}}\mathbf{D}}\mathbf{H}^{\mathrm{T}}\mathbb{R}\mathbb{L}^{\dagger}\begin{bmatrix}1\\0\end{bmatrix} = \frac{\hbar}{2}\frac{\mathbf{H}^{\mathrm{T}}\mathbb{L}\begin{bmatrix}1\\0\end{bmatrix}}{\mathbf{H}^{\mathrm{T}}\mathbb{L}\begin{bmatrix}0\\1\end{bmatrix}}. \tag{60}$$

It is useful to have these spectral densities in different normalizations. The connection between them is:

$$S^x = S^F |\chi_{xx}^{\text{eff}}|^2, \tag{61}$$

$$S^h = S^F \left(\frac{2}{mL\omega^2}\right)^2. \tag{62}$$

B Optimal spectral density

As we know from the appendix A, renormalized output for one pump is:

$$\hat{\mathcal{O}}^F(\omega) = \frac{\hat{\mathcal{X}}}{\chi_{xx}^{\text{eff}}(\omega)} + \hat{\mathcal{F}}(\omega) + G(\omega). \tag{63}$$

Thus total output for n pumps can be combined optimally with filtering functions K_i:

$$\hat{\mathcal{O}}^F(\omega) = \sum_{i=1}^{n} K_i \hat{\mathcal{O}}^F, \tag{64}$$

where

$$\sum_{i=1}^{n} K_i = 1. \tag{65}$$

Resulting spectral density is:

$$S^F = \sum_{i,j=1}^{n} K_i K_j^* S_{ij}, \tag{66}$$

where spectral densities are:

$$S_{ij} = \frac{S_{\mathcal{X}\mathcal{X}}^{ij}}{|\chi_{xx}^{\text{eff}}|^2} + S_{\mathcal{F}\mathcal{F}} + \frac{S_{\mathcal{X}\mathcal{F}}^{i}}{\chi_{xx}^{\text{eff}}} + \frac{S_{\mathcal{X}\mathcal{F}}^{j,*}}{\chi_{xx}^{eff,*}}, \tag{67}$$

and

$$S_{\mathcal{X}\mathcal{X}}^{ij} = \delta_{i,j} \frac{\hbar}{4\gamma m J_i} \frac{1}{\left|\mathbf{H}_i^{\mathrm{T}} \mathbb{L}_i \begin{bmatrix}1\\0\end{bmatrix}\right|^2}, \tag{68}$$

$$S_{\mathcal{F}\mathcal{F}} = \sum_{i=1}^{n} \gamma_i m \hbar J_i \begin{bmatrix}1\\0\end{bmatrix}^{\mathrm{T}} \mathbb{L}_i \mathbb{L}_i^{\dagger} \begin{bmatrix}1\\0\end{bmatrix}, \tag{69}$$

$$S_{\mathcal{X}\mathcal{F}}^{i} = \frac{\hbar}{2} \frac{\mathbf{H}^{\mathrm{T}} \mathbb{L}_i \begin{bmatrix}1\\0\end{bmatrix}}{\mathbf{H}^{\mathrm{T}} \mathbb{L}_i \begin{bmatrix}0\\1\end{bmatrix}}. \tag{70}$$

To find optimal filtering function we have to equal all partial derivatives to zero (taking into account normalization (65)):

$$\frac{\partial S^F}{\partial K_i} = \sum_{j=0}^{n-1} K_j^* (S_{ij} - S_{ni} - S_{in} + S_{nn}) + S_{in} - S_{nn} = 0. \tag{71}$$

Solution of this linear system gives us n optimal filtering functions that minimize the total spectral density.

C Analysis of the response function

Function $\mathcal{K}$ has complex poles that are complexly conjugated:

$$\mathcal{K}(\omega) = \frac{MJ\delta}{(\gamma - i\omega)^2 + \delta^2} = \frac{M}{2}\left(\frac{iJ}{i\omega - (\gamma - i\delta)} - \frac{iJ}{i\omega - (\gamma + i\delta)}\right). \tag{72}$$

In other words, we have sum of two terms with complexly conjugated pole $y = \gamma - i\delta$ and pure imaginary residuals $g = iJM/2$ (as long as the power should be real):

$$\mathcal{K}(s) = \frac{g}{s - a} + \frac{g^*}{s - y^*}. \tag{73}$$

Let's consider the general case: for the infinite number of springs we have continuum of poles in complex plane, thus we can assume that each poles depends on some parameter θ and instead of summation over springs we should write the integral:

$$\mathcal{K}_{\text{total}} = \int_0^{2\pi} \frac{ig(\theta)}{s - y(\theta)} d\theta. \tag{74}$$

Now we should make some restrictions on this integral:

- $g(\theta)$ is real because it is a power,
- $y(\theta) = -y(\theta)^*$ because complex poles are complexly conjugated pairs,
- $g(\theta) = -g(\pi - \theta)$ because residuals are complexly conjugated pairs as well

The other assumption is that y forms closed contour in the complex plane. Then integration over parameter can be changed to the integration over this contour

$$\mathcal{K}_{\text{total}} = \oint \frac{ig(y)}{dy/d\theta} \frac{dy}{s - y}. \tag{75}$$

As we know from Cauchy integral formula for any holomorphic function f that projects open subset U on the complex plain $\{f : U \to \mathbb{C}\}$:

$$f(a) = \frac{1}{2\pi i} \oint_C \frac{f(z)}{z - a} dz \tag{76}$$

for every $a \in D$, where $D \subset U$ and $C = \partial D$.

Our aim is to achieve $\mathcal{K}_{\text{total}}(s) = p(s)$ where $p(s)$ is a real polynomial function of s in general. Let's first consider particular case when $p(s) = As^2 + B$. Using Cauchy equation:

$$Ay^2 + B = \frac{-2\pi g(y)}{dy/d\theta}. \tag{77}$$

Now write two equations for real and imaginary part $y = a + ib$:

$$(Aa^2 - Ab^2 + 2Aiab + B)da + i(Aa^2 - Ab^2 + 2Aiab + B)db = i\epsilon d\theta. \tag{78}$$

Let's say for simplicity $A = 1, B = 1$

$$\begin{cases} (1 + a^2 - b^2)da - 2abdb = 0, \\ 2abda + (a^2 - b^2 + 1)db = g(\theta)d\theta. \end{cases} \tag{79}$$

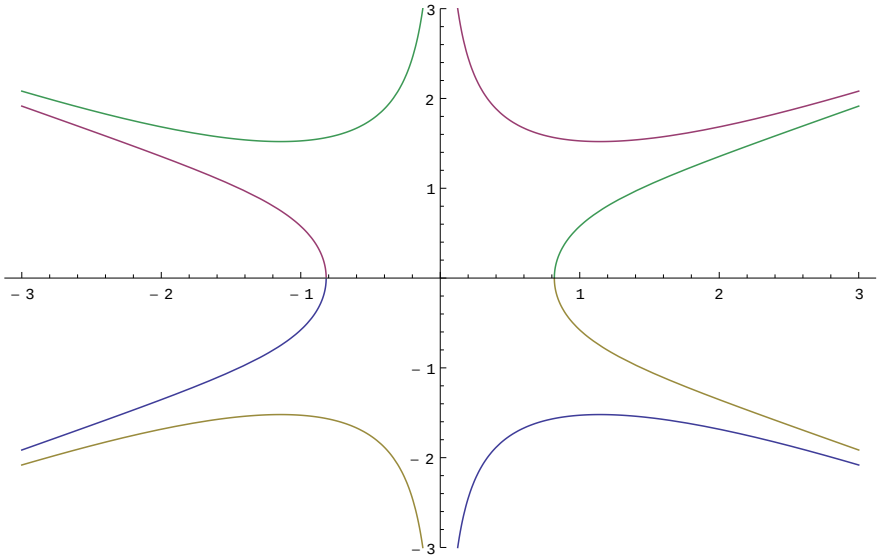

Figure 5: Poles trajectories on the complex plane

First equation gives us:

$$d(a+\frac{1}{3}a^3)-(b^2da+adb^2)=0 \quad \Rightarrow \quad a+\frac{a^3}{3}-ab^2=C\equiv const. \tag{80}$$

Or, in other words, the complex part depends on the real one as:

$$b=\pm\sqrt{1\pm\frac{C}{a}+\frac{a^2}{3}}. \tag{81}$$

which gives us the trajectories shown in Fig. 5.

Obviously this contour is not closed, but it can be shown that if we artificially close the loop the error will converge to zero. Let's prove it for the second order polynomial and then in general. Distance between two branches $b_{1,2}$ is

$$\rho=|b_1-b_2|^2=1+\frac{C}{a}+\frac{a^2}{3}+1-\frac{C}{a}+\frac{a^2}{3}-2\sqrt{(1+\frac{a^2}{3})^2-\frac{C^2}{a^2}}=2\left(1+\frac{a^2}{3}-\sqrt{(1+\frac{a^2}{3})^2-\frac{C^2}{a^2}}\right). \tag{82}$$

Solving minimization problem:

$$\frac{\partial\rho}{\partial a}=2\left(\frac{4a}{3}-\frac{1}{2}\frac{2(1+a^2/3)2a/3+2C^2/a^3}{\sqrt{(1+\frac{a^2}{3})^2-\frac{C^2}{a^2}}}\right)\approx(1+\frac{a^2}{3})\frac{C^2}{a^2(1+\frac{a^2}{3})^2}=\frac{C^2}{a^2(1+\frac{a^2}{3})}. \tag{83}$$

Though it is never equals to zero, it approaches zero as fast as 4th order of a that proves initial assumption.